

**Development of the SmartAnswer Demonstrator  
a Didactic Wind Tunnel for Aeroacoustic Applications\***

Tamaro, S.; Zamponi, R.; Schram, C.

**DOI**

[10.2514/6.2022-3060](https://doi.org/10.2514/6.2022-3060)

**Publication date**

2022

**Document Version**

Final published version

**Published in**

28th AIAA/CEAS Aeroacoustics Conference, 2022

**Citation (APA)**

Tamaro, S., Zamponi, R., & Schram, C. (2022). Development of the SmartAnswer Demonstrator: a Didactic Wind Tunnel for Aeroacoustic Applications . In *28th AIAA/CEAS Aeroacoustics Conference, 2022* Article AIAA 2022-3060 (28th AIAA/CEAS Aeroacoustics Conference, 2022). American Institute of Aeronautics and Astronautics Inc. (AIAA). <https://doi.org/10.2514/6.2022-3060>

**Important note**

To cite this publication, please use the final published version (if applicable).  
Please check the document version above.

**Copyright**

Other than for strictly personal use, it is not permitted to download, forward or distribute the text or part of it, without the consent of the author(s) and/or copyright holder(s), unless the work is under an open content license such as Creative Commons.

**Takedown policy**

Please contact us and provide details if you believe this document breaches copyrights.  
We will remove access to the work immediately and investigate your claim.



# Development of the SmartAnswer Demonstrator: a Didactic Wind Tunnel for Aeroacoustic Applications\*

S. Tamaro<sup>†</sup> and R. Zamponi<sup>‡</sup> and C. Schram<sup>§</sup>  
*von Karman Institute for Fluid Dynamics, Sint-Genesius-Rode 1640, Belgium*

A small didactic wind tunnel demonstrator has been designed and manufactured at the von Karman Institute for Fluid Dynamics to illustrate the physical principles at stake in flow-induced noise generation, offer an audible perception of the effectiveness of noise-mitigation strategies, and serve as a practical test bench for aeroacoustic education and research. Seven mitigation technologies are embedded in a single facility, which addresses the noise generation by an airfoil, noise propagation in a duct, and noise transmission through a flexible panel. A challenging objective of this facility was to offer a perceptible impression of various aeroacoustic noise mechanisms at low flow speeds and a live assessment of the effectiveness of the noise-reduction technologies. Different approaches combining multiple microphones, advanced signal-processing techniques, and real-time audio feedback have been implemented to this end. The results establish that the demonstrator enables a clear perception of the effectiveness of the noise-mitigation technologies. The facility is also suitable for fast and inexpensive preliminary investigations of future noise-reduction concepts, taking advantage of rapid prototyping techniques.

## I. Introduction

THE unavoidable growth in air and ground traffic, the desired increase of wind energy, the constant spread of cooling and ventilation systems, etc., require new technologies to limit the noise exposure in our homes and workplaces. Indeed, the negative impact of noise on our quality of life and health is well known. The elaboration of improved noise-mitigation strategies is therefore essential to limit noise to the acceptable levels that have been defined in many sectors of activity. For this purpose, new materials and technologies are being actively researched, leading the way to innovative products by a new generation of young scientists, researchers, and entrepreneurs.

Both aspects, technological progress and training of young researchers, are part of the core mission of Marie Skłodowska Curie Actions (MSCA), funded by the European Commission. The MSCA Innovative Training Networks (ITN) SMARTANSWER\* has been researching, developing, and promoting innovative flow and noise control approaches for multiple applications, such as wind turbines, aircraft, and air conditioning systems, for the building and automotive industries. This project has brought together young researchers and industrial stakeholders with the common goal of accelerating the development of novel noise-reduction technologies.

One of the key achievements of the project has been the design of a didactic demonstrator, which has several purposes: (i) communicating the outcomes of the research to a broad audience, including nonspecialists; (ii) stimulating the interest of younger generations toward scientific studies; and (iii) serving as a small laboratory facility for the training of undergraduate or Masters-level young researchers. The first objective is addressing the issue of the growing complexity of scientific research, resulting in its disconnection from the broader public, although the latter is financing this research. The public acceptance of the governmental scientific policies is, here, at stake. The second objective considers a longer perspective and attempts to increase the interest of young people in scientific studies with the aim of preserving the competitiveness of the European area in the decades to come. The last objective speaks for itself and is meant to guarantee the continuous maintenance and upgrade of the facility over the years. The didactic demonstrator concept is not new: Hawkinson and Anderson [2] have pointed out the benefits of a small flight demonstration wind tunnel as an outreach tool and, especially, as an active learning environment for students. A miniature wind tunnel has

\*Parts of this paper are included in [1].

<sup>†</sup>Research Engineer, Environmental and Applied Fluid Dynamics Department, simone.tamaro1@gmail.com.

<sup>‡</sup>Postdoctoral Researcher, Environmental and Applied Fluid Dynamics Department, riccardo.zamponi@vki.ac.be, AIAA Member

<sup>§</sup>Professor, Environmental and Applied Fluid Dynamics Department & Aeronautics and Aerospace Department, christophe.schram@vki.ac.be, AIAA member

\*Smart mitigation of flow-induced acoustic radiation and transmission for reduced aircraft, surface transport, workplaces, and wind energy noise, available at <https://www.h2020-smartanswer.eu/> (Last viewed on 31<sup>st</sup> January 2022).

also been described numerically and experimentally by Duran et al. [3], who developed it to assist the undergraduate students of flight control. But to the authors' knowledge, the development of a didactic aeroacoustic demonstrator, which enables the user to experience live the noise-reduction technologies, has never been reported in the literature.

The design of the small aeroacoustic wind tunnel, which is described in this paper, is the outcome of an intensive collaboration between the participants of the consortium [4]. The SMARTANSWER demonstrator implements the noise-reduction technologies, which were investigated by the young researchers recruited in the project. Whereas the noise-mitigation concepts and the main research outcomes of those fellows are summarized below with adequate referencing to their publications, the present paper is focused on the development of the wind-tunnel platform itself and the techniques that were specifically studied to enable the *in situ* hearing of flow-induced noise-generation, propagation, and transmission mechanisms and their attenuation. Here, the purpose is to present the demonstrator's design and discuss its potential as an outreach tool and active learning station.

The document is structured as follows. Section II briefly outlines the state-of-the-art of some of the main noise-reduction technologies embedded in the demonstrator. Section III presents the design of the demonstrator facility. In Sec. IV the main results are shown and their educational potential is discussed, whereas the conclusions are drawn in Sec. V.

## II. Noise-mitigation technologies

In this section, aerodynamic-noise reduction is considered, following three different approaches: by acting on its source, the way it propagates in a duct, and the way it is transmitted through a flexible panel.

### A. Reduction of noise at the source

When the flow interacts with a solid body such as an airfoil, different noise-generation mechanisms occur. In the case of a fixed airfoil, the sources of the aerodynamic noise can be typically divided into self-noise and interaction noise. The tip noise and trailing-edge noise are two examples of self-noise. The trailing-edge noise originates when the turbulent structures, which develop in the airfoil boundary layer above a critical Reynolds number, are advected over the trailing edge. The tip noise occurs when the tip vortex, induced by a pressure difference between the pressure and suction sides, interacts with the blade tip. The turbulence-interaction noise takes place when the incoming turbulent structures are distorted in the proximity of the leading edge of a blade or wing. The noise generation can be mitigated at the source by modifying the geometry of the specific areas, such as the leading edge and trailing edge of a wing, or introducing porous materials.

**Serrations** Serrations are wavy-shape inserts that can be installed at both edges of a wing or blade profile. The leading-edge serrations have been applied to isolated profiles and fan blades [5, 6]. The oblique edge on a leading-edge serration hill creates a destructive interference of the scattered surface pressure [7, 8], resulting in a noise reduction in targeted frequency ranges. The wavy design is correlated directly with the turbulence integral length scale so that an optimum serration wavelength equal to four times the integral length scale has proven to achieve maximum sound power reductions [9]. Serrations can also be applied to passively mitigate trailing-edge noise [10]. The noise-reduction mechanism, in this case, is linked to the destructive interference occurring between pressure waves that are scattered at the edges [11].

**Porous materials** Similar to serrations, porous materials can be integrated into the structure of an airfoil to mitigate both self-noise [12–14] and turbulence-interaction noise [15–18]. At the leading edge, one possible mitigation mechanism for the turbulence-interaction noise is related to the damping of the deformation that is experienced by the turbulent vortices impinging on the airfoil surface. This phenomenon results in a less efficient conversion of their kinetic energy into sound [19]. Moreover, the communication between the pressure and suction sides mitigates the noise emissions by decreasing the pressure jump across the surface, thereby attenuating the associated dipole. A more detailed discussion on the physical mechanisms is provided by Paruchuri et al. [20]. At the trailing edge, the porosity reduces the self-noise by mitigating the acoustic impedance discontinuity in this region [21].

**Over-the-rotor liners** An important noise component in the turbofan engines is that which is generated by the interaction of the flow with the rotor blades and stator vanes. In particular, the tip clearance is a relevant source of the self-noise because the pressure difference between the two sides of a blade starts a tip-leakage vortex, which interacts

with the blade tip edge [22, 23]. To this end, the over-the-tip liners (OTLs) have been investigated during the past decades as a technology with the potential to attenuate the fan noise in turbofan engines [24]. This concept consists of treating the casing surrounding the fan blades by fitting an acoustic liner. Due to the close vicinity to the fan-blade tip, the noise-mitigation mechanism of the OTLs is typically attributed to a modification of the source itself combined with the conventional attenuation of the acoustic waves that propagate over the liner.

**Rod vortex generators** Flow separation is a common scenario for many technological applications. It occurs at high inflow incidence angles and decreases the aerodynamic performance, stall, fatigue, and low-frequency noise generation [25]. The vortex generators are passive flow-control devices, which are capable of delaying the flow separation by generating the streamwise vortices, which transfer the high-momentum fluid to the core of the boundary layer [26]. The novel design of the rod vortex generators (RVGs) has been introduced by Doerffer et al. [27] and uses small inclined cylinders as control devices. The effect of the RVGs on the aerodynamic noise is still a topic of active research. Indeed, the turbulence generated by the RVGs is convected downstream and scattered at the trailing edge with a risk of regenerating noise, thereby deteriorating the expected benefits of preventing a loud, low-frequency stall noise.

## B. Noise propagation

The acoustic passive and active liners are technologies that have proved to successfully mitigate the duct-noise propagation [28, 29]. On the one hand, the former act on a wide range of frequencies and do not require energy to operate. However, their main limitation is that they cannot adapt to multiple scenarios due to the fixed geometry and materials. On the other hand, the latter provide a similar performance with higher flexibility and can be tuned in real-time.

**Passive liners** Passive liners are made of a perforated plate, coupled to a cavity on one side, and can be reactive or dissipative, depending on the nature of this cavity. The reactive liners are backed by a resonating honeycomb structure, whereas the dissipative liners are backed by porous, sound-absorbing materials. The passive liners reduce far-field noise by absorbing acoustic energy and can be tuned to target virtually any frequency range [30]. The performance of a passive liner depends on the different parameters such as the perforation size, perforation rate, thickness, and mounting conditions [30].

**Active liners** Semi-active impedance control offers a promising alternative to overcome the lack of versatility of the passive liners [28]. An active liner consists of an array of electroacoustic cells, made by a loudspeaker (the actuator) placed in the center of the cell, and one or more microphones (the sensors) fitted around it. By controlling the electrical current in the loudspeaker coil with a programmable digital processor, it is possible to change the loudspeaker dynamics based on the microphone measurements and reproduce the desired relationship between the actuator displacement and local averaged pressure [29].

## C. Noise transmission

The use of lightweight materials has become crucial to several engineering applications as a result of ecological trends. Nonetheless, the light designs exhibit worse noise, vibration, and harshness behavior, and novel low-mass and compact solutions are required to improve it. With this regard, locally resonant metamaterials can create frequency zones of strong vibration and/or noise attenuation, i.e., stop bands, by reducing the flow-induced vibrations of flexible structures and the consequential transmission of noise [31, 32]. The technology consists of a flat plate onto which the resonant structures, called resonators, are glued. The installation pattern of these units, along with their dimensions, determines the stop band behavior [33].

## III. Design of the demonstrator wind tunnel

The objective pursued with this demonstrator is to offer a live, ideally audible, experience of the flow-induced noise and its mitigation, thanks to the aforementioned technologies, while being sufficiently compact to be transportable and exhibited in schools, universities, science fairs, etc. A relatively low maximum flow speed is permitted in these conditions, which significantly limits the noise-production amplitude. For this reason, it has been decided to amplify the noise measured by the near-field microphones and reinject it through a loudspeaker to enable a live audio hearing.

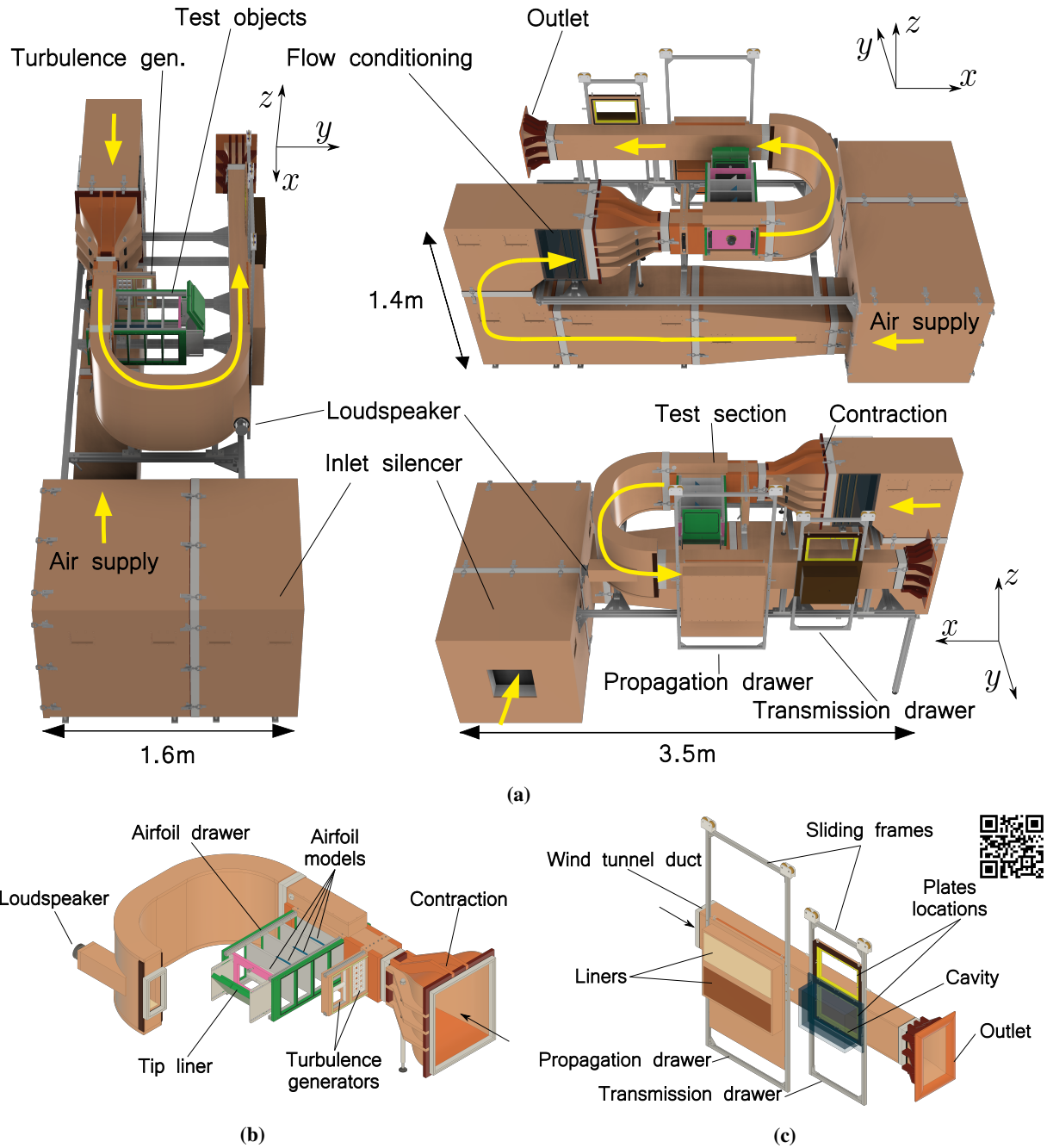


**Fig. 1 Computer-aided design (CAD) views of the demonstrator wind tunnel facility: (a) general overview, (b) airfoil drawer, (c) propagation and transmission drawers. Arrows indicate the flow direction. A video describing the architecture and the operation of the facility is available online and can be accessed by scanning the QR code embedded in the figure.**

The demonstrator consists of a miniature open-loop wind tunnel made of interlocking wooden elements, which can be easily disassembled. The facility features manually operated drawers to quickly shift between the different airfoils and noise-reduction technologies and an amplification circuit to provide the best possible perception. This solution offers the benefit of adapting the audio output to the background noise level of the demonstration environment.

## A. Aerodynamic and acoustic design

The wind tunnel has been designed to operate at a subsonic target point of  $20 \text{ m s}^{-1}$  in an open-loop configuration. Figure 1 presents the different elements and views of the facility. A fairly silent centrifugal fan model G3G250-KR17-I5, provided by EBM-Papst [34], supplies the required volumetric flow rate. The fan is equipped with an alternate current single-phase M3G084-DF motor. The fan intake is connected to a silencer box containing a labyrinth of melamine-foam panels. The fan outlet discharges into a straight horizontal duct section terminated by a vertical U-turn, and also fitted with 0.1 m melamine-foam panels on its four sides. The U-turn leads to a flow-conditioning settling chamber, which includes a honeycomb flow straightener and three turbulence screens. A seventh-order polynomial contraction with an area ratio of 10 leads to the 0.2 m (height)  $\times$  0.1 m (span) test section.

A drawer with five compartments, hosting different airfoils, can slide through the test section along the spanwise direction to quickly change the investigated configuration and assess the noise attenuation gained with the serrations, porous materials, etc. This element is shown in detail in Fig. 1b. The different inflow qualities can be obtained by sliding a second drawer, located approximately 0.2 m upstream of the test section, containing either (i) an empty section for clean inflow conditions, leading to trailing-edge noise; (ii) a coarse grid generating homogeneous turbulence for broadband turbulence-interaction noise; or (iii) a 0.01 m-diameter cylindrical rod, inducing a periodic vortex shedding for the quasi-tonal turbulence-interaction noise [35].

The flow velocity in the facility is measured with a Validyne pressure sensor model DP15 (Validyne Engineering, Northridge, CA, United States) plugged into a CD15 carrier demodulator and connected to the inlet and outlet of the convergence. The device has been calibrated using a Betz-type water manometer (ACIN instrumenten, Rijswijk, the Netherlands) and is characterized by an uncertainty of 0.5 %. In the clean configuration, the hot-wire anemometry measurements indicated turbulence intensities on the order of 0.5 %. The coarse grid has a thickness of 0.01 m and square openings of 0.02 m side length, generating turbulence intensities that are estimated around 20 % at the level of the airfoil leading edge. The bars of the grid are covered with 0.02 m of melamine foam on their upstream and downstream faces to minimize the grid self-noise.

Downstream from the test section, a smooth U-turn guides the flow toward a straight duct of approximately 1.6 m in length. A loudspeaker is embedded into the downstream corner to reinject the airfoil noise after amplification toward the final straight duct. The top and bottom walls of the U-turn are acoustically treated with melamine foam to minimize the risks of an audio feedback loop between the loudspeaker and test-section microphones. This feature can be observed in Fig. 1b.

Two vertical drawers, sliding vertically, are installed along the final straight duct. Both of the elements are visible in Fig. 1c. The upstream element (*propagation drawer*) allows a passive or active acoustic liner to be installed by sliding one vertical solid sidewall. The propagation drawer is 0.545 m long in the streamwise direction and enables flushing a liner on the whole 0.2 m height of the sidewall of the duct. A lower transmission of the airfoil noise can be appreciated at the outlet of the duct by switching between the solid wall and passive/active liners.

The downstream vertical drawer (*transmission drawer*) is in place to demonstrate the noise transmission. One sidewall is free to slide to present either a thin steel plate or an architected metamaterial panel. The mechanism has a streamwise length of 0.4 m and transmits the sound propagating in the duct toward a rectangular backing cavity made of Plexiglass walls, which is instrumented with a microphone. Switching from the steel panel to the metamaterial panel is meant to yield a reduced transmission toward the Plexiglass cavity.

Finally, the flow exits the facility through an outlet horn with an area ratio of approximately 3.9 to reduce the relative pressure loss and radiate the noise toward the audience. The assembled rig has a total height of 2.0 m, width of 1.6 m, and length of 3.5 m, and can be easily disassembled using toggle latches and transported in a small truck.

## B. Implementation of the noise-reduction technologies

The technologies for noise reduction at the source are installed in the airfoil drawer. The technologies for the mitigation of the duct-noise propagation are located in the liner drawer. The metamaterial for attenuating the noise transmission is mounted in the transmission drawer.

### 1. Airfoil drawer

Five different wing profiles are installed in the airfoil drawer: one reference airfoil and four variants featuring the noise-mitigation technologies listed in Sec. II.A, separated by Plexiglas walls. The models are aligned and coupled to a cylindrical axis, which can be rotated to set a common angle of attack, with an estimated uncertainty of  $\pm 1^\circ$  due to the manufacturing tolerances. The reference baseline airfoil is a National Advisory Committee for Aeronautics NACA-0012

profile with a chord of 0.12 m. All of the airfoils have been three-dimensionally printed in a polycarbonate material using a powder-based printing technique, and occupy the full-span 0.1 m of the test section, at the exception of the airfoil meant to demonstrate the tip-gap noise reduction, for which a gap of 0.005 m has been implemented. For the clean inflow conditions, the baseline airfoil has been tripped at  $x/c = 0.1$  to induce the transition from the laminar to turbulent boundary layer. Figure 2 illustrates the three-dimensional (3D) models of the airfoils installed in the demonstrator.

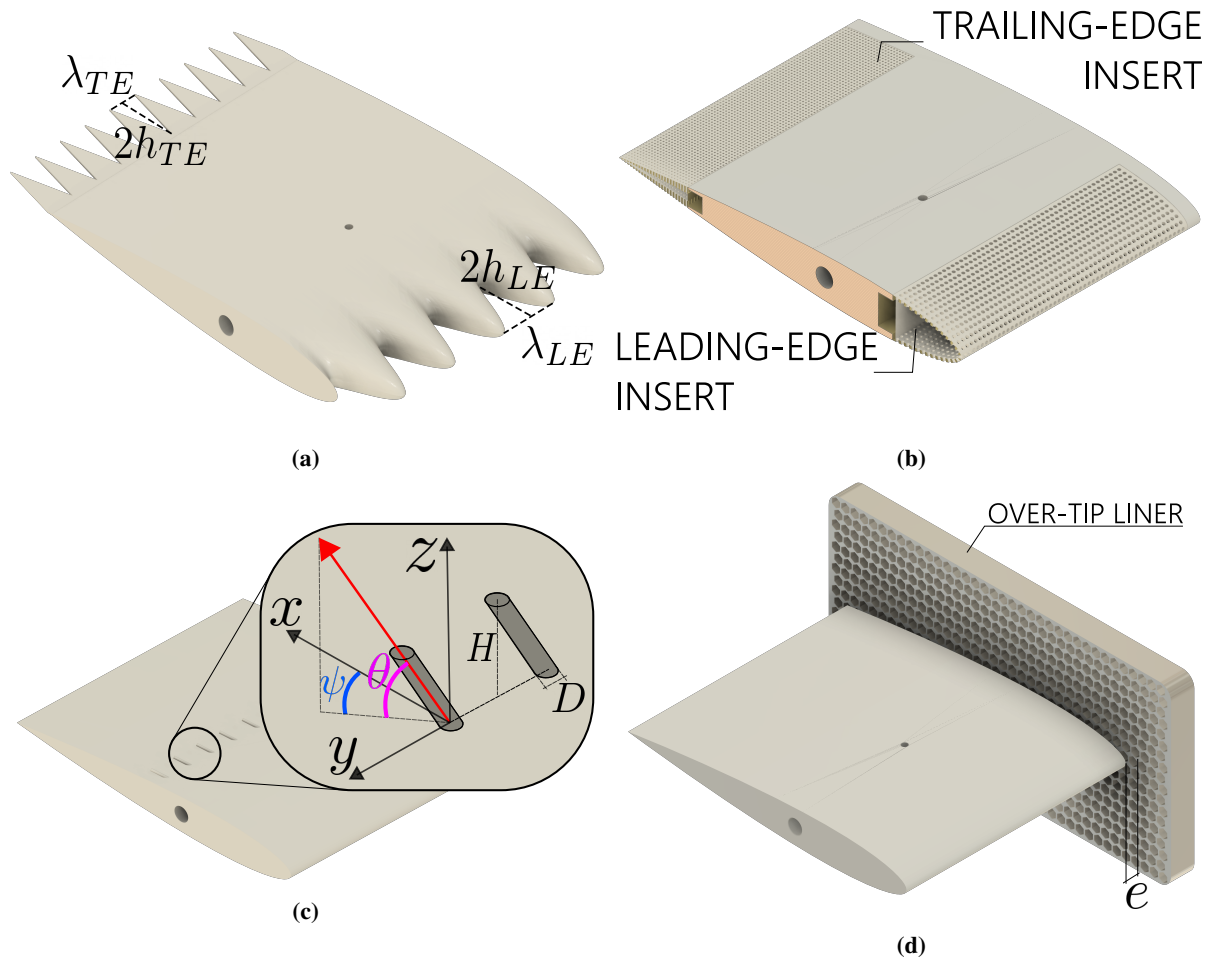


**Fig. 2 Test objects for the noise reduction at the source: (a) serrated airfoil, (b) section view of the porous airfoil, (c) RVG airfoil and parameters, (d) tip-gap airfoil and OTL. The baseline is a symmetric NACA-0012 profile with a chord of 0.12 m and a span of 0.1 m.**

**Serrations** The sinusoidal leading-edge serrations have been designed following the guidelines mentioned in Sec. II.A, preserving a total surface of the airfoil platform equal to that of the reference airfoil. The peak-to-trough amplitude of the serrations is  $2h_{LE} = 0.02$  m, equal to the wavelength  $\lambda_{LE} = 0.02$  m.

At the trailing edge, sawtooth serrations have been designed based on an the estimated boundary-layer thickness  $\delta_{99} = 0.005$  m, measured through hot-wire anemometry. The peak-to-trough amplitude is  $2h_{TE} = 4\delta_{99} = 0.02$  m, for a wavelength  $\lambda_{TE} = 0.01$  m, following the guidelines of Gruber et al. [36]. The dimensions of  $h_{TE}$  and  $\lambda_{TE}$  yield a serration angle of  $76^\circ$ , matching the recommendations of Howe [37]. The thickness of the serrations of 5 mm is the minimum imposed by the 3D printing technique.

**Porous materials** The porous model is equipped with perforated leading-edge and trailing-edge inserts. The perforation allows the incoming flow to penetrate the airfoil. The internal volume of the perforated inserts is filled with

steel wool to prevent acoustic resonance. The present design is based on the work of Teruna et al. [38] and Rubio Carpio et al. [39]. At the leading edge, the perforations are locally perpendicular to the surface with a hole diameter of 1 mm, and center-to-center separations of 1.5 mm and 1.8 mm in the spanwise and streamwise directions, respectively. The surface porosity is 73 %. The outer structure is 1 mm thick, and the leading-edge insert extends up to 20 % of the chord.

The same dimensions for the outer structure also characterize the trailing-edge insert. The perforations are perpendicular to the chord line with hole diameters of 0.5 mm, and the inter-hole separation is 1 mm in the streamwise and spanwise directions. This design yields a surface porosity equal to 20 %. Underneath the perforations, the prismatic cavity has a height of 2.5 mm at the solid-porous junction and a height of 0.5 mm at the trailing edge. The perforation channels are longer near the junction and gradually become shorter toward the trailing edge. This treatment effectively leads to a streamwise variation of the flow resistivity of the perforated trailing edge, intended to minimize the scattering intensity at the solid-porous junction and, subsequently, the high-frequency noise increase. However, issues related to the tolerance of the 3D printing process did not allow for the successful manufacturing of the trailing-edge porosity. In particular, the high number of occluded perforations at the trailing edge compromises the permeability - and, therefore, the noise-reduction potential - of the insert.

**RVGs** Figure 2c shows the geometrical parameters that define one RVG. Each component has a diameter of  $D = 1$  mm, corresponding to 20 % of the estimated boundary layer thickness  $\delta_{99} = 5$  mm at the VG location, and a height (along  $z$ ) of  $H = 2.25$  mm, corresponding to 45 % of  $\delta_{99}$ . A total of ten RVGs are installed along the span at a chordwise location  $x/c = 0.5$  and with a spanwise separation of  $10D$ . The inclination of a RVG is determined by two angles  $\theta$  and  $\psi$  as indicated in Fig. 2c. The angle relative to the  $xy$  plane is  $\theta = 45^\circ$ , while the angle relative to the  $xz$  plane is  $\psi = 30^\circ$ . The RVGs have been glued into dedicated slots on the suction side of a baseline airfoil model.

**OTL** The set-up of the OTL in the demonstrator is based on the wind tunnel experiments conducted by Palleja-Cabre et al. [22], in which the rotor and OTL are represented by a static airfoil with its tip located over a flat plate containing a flush-mounted liner insert and separated from the airfoil tip by a small gap of 5 mm. On the exterior wall of the test section, two hinges allow easy swapping of two different panels, i.e., a hard wall or a liner in the over-tip position with a surface of  $0.21 \text{ m} \times 0.12 \text{ m}$ . An elastic O-ring is used to seal the panels to the test section. The geometric design of the liners is based on the point source prediction model by Palleja-Cabre et al. [22], adequately tuned for the airfoil chord and flow speed of the demonstrator. The mitigation technology is a 10 mm thick, one degree of freedom (passive) liner, consisting of a cubic aluminum honeycomb structure, with a wire mesh on the flow side.

## 2. Propagation drawer

**Passive liner** The passive liner is dissipative and consists of a micro-perforated plate with a porous cube installed behind it. The perforated plate is designed using Guess's model [40], targeting a frequency range around 1.5 kHz. The porous melamine-foam cube operates at a wider frequency range, according to the properties of the porous medium.

**Active liner** The active liner consists of an array of twelve Monacor SPX-30M loudspeakers (Monacor International, Bremen, Germany) and twelve electret microphones, installed on a mechanical frame and covered by a wire mesh. Two different acquisition boards (three for the loudspeakers and three for the microphones) and one controller are required to operate the device. The dynamic response of the loudspeakers is controlled with a feed-forwarded control loop. The target impedance is expressed as a function of three control parameters  $\mu_r$ ,  $\mu_m$ , and  $\mu_c$ , which can be used to modify the effective mass, resistance, and compliance of the loudspeakers, respectively [28]. The optimum values of  $\mu_r = 0.2$  and  $\mu_m = \mu_c = 0.5$  yield a band-filter behavior centered at approximately 310 Hz and expected reduction higher than 6 dB.

## 3. Transmission drawer

The metamaterial panel measures 200 mm (height)  $\times$  300 mm (streamwise length)  $\times$  0.5 mm (thickness), and features 90 resonators with a thickness of 4 mm and an average resonance frequency of  $1926 \text{ Hz} \pm 8 \text{ Hz}$ . They are installed in a rectangular pattern with a streamwise separation of 28 mm and upwash separation of 20 mm to target the first transversal axial mode of the cavity estimated at 1.3 kHz. The resonators are designed as cantilever beams with rectangular support of  $20 \text{ mm} \times 28 \text{ mm}$  and made of polymethyl methacrylate. Further details on the design of these devices can be found in [33].

### C. Amplification of the airfoil noise

The near-field noise emitted by the airfoil needs to be amplified to provide a live audio experience, given the low flow velocities. However, a single microphone placed close to the airfoil in the test section would not be sufficient as it would also pick up the pressure fluctuations associated with the flow itself, in addition to the residual noise of the fan and any other background noise.

An array of microphones was used to extract the noise emitted by the airfoil from the background noise. Two sets of four microphones are immersed in a 0.1 m-thick block of melamine foam fitted within the upper and lower walls of the test section. The purpose of these patches of foam, covered by a tensioned metallic fine cloth, is to dampen out the vertical transverse modes that would otherwise yield a tonal spectrum and alter the perception of the broadband noise emitted by the airfoil.

Each lower/upper set of microphones is recessed by about 7 mm inside the melamine foam to decrease the contribution of the lower/upper wall turbulent boundary layer to the measured signal. Two microphones are placed over a line aligned with the airfoil leading edge, and two microphones are facing the trailing edge. The spanwise separation between each pair of microphones is about 0.04 m, estimated enough to yield a decorrelation of the pressure fluctuations associated with the boundary layers while preserving the correlation of the acoustic pressure radiated by the airfoil. Based on this assumption, the signals of each pair of microphones are averaged in real-time to increase the signal-to-noise ratio.

The averaged signals from the sets of microphones facing each other across the test section are then subtracted. This procedure is meant to further increase the signal-to-noise ratio because the acoustic field radiated by the airfoil is, in the first approximation, of dipolar nature at low enough frequencies [41]. Therefore, the signals corresponding to the airfoil acoustic field at the upper and lower microphones should be in anti-phase, whereas the background noise is not expected to be. Thus, at the low frequencies, the residual fan noise transmitted to the test section is expected to appear as plane waves in the test section and should be canceled in the subtraction.

The microphones are cheap electrets, of the brand Knowles and model FG23329-P07 (Knowles, Itasca, IL, United States), with a diameter of 2.59 mm, a frequency response of  $\pm 3$  dB in a range between 100 Hz and 10 kHz, and a typical uncertainty of  $\pm 1$  dB. All of the sensors have been calibrated in amplitude and phase. The signals acquired by the electret microphones are processed as mentioned above and then sent to an amplifier with an adjustable gain and fed to an analog input module NI-9205 (National Instruments, Austin, TX, United States). The input and output modules are installed in a CompactDAQ NI cDAQ-9174 chassis (National Instruments, Austin, TX, United States). The input data are processed using NI LabVIEW (National Instruments, Austin, TX, United States) and can be either stored or played by a Monacor SPH-75/8 loudspeaker (Monacor International, Bremen, Germany) using an analog output module NI-9263 (National Instruments, Austin, TX, United States), after amplification by a Monacor AKB-60 amplifier (Monacor International, Bremen, Germany), leading to the loudspeaker.

An interface has been developed to permit choosing which of the leading- or trailing-edge microphones are amplified to freeze the multiple sound pressure spectra on the screen for comparison as well as apply the A-weighting [42]. The bandpass filtering of the signal is also implemented and can be tuned appropriately to enhance the perception of the resulting acoustic behavior. The sampling frequency is 25.6 kHz in the acquisition mode and reduced to 12.8 kHz for the amplification.

The measurements of the noise propagation and transmission have been performed employing a B&K Type 4938 1/4-in microphone (Bruel & Kjaer, Nærum, Denmark). A NEXUS Conditioning Amplifier type 2692-C (Bruel & Kjaer, Nærum, Denmark) is used to amplify the signal acquired by the microphone and feed it to the analog input module. The sampling frequency, in this case, is set to 12.8 kHz. To measure the effectiveness of the liners for noise propagation, the B&K microphone is placed at the outlet of the facility at a distance of 0.3 m from its center, lying in the horizontal plane, whereas to estimate the noise transmission, it is located at the center point of the backing cavity, flush with the inner surface.

The acoustic spectra presented in Sec. IV are computed using the Welch method with a Hanning window size of  $2^{11}$  sampling elements and a frequency resolution of 12.5 and 6.5 Hz for the data acquired with the electret microphones and B&K microphone, respectively. The acquisition time is set to 30 s for the noise at the source, 12 s for the noise propagation, and 10.5 s for the noise transmission.

## IV. Commissioning of the facility

The quantitative results below demonstrate that the facility developed in this work permits a qualitative perception of the flow-induced noise and its mitigation.

### A. Noise reduction at the source

The following results were obtained for the free-stream velocities between  $U_\infty = 10 \text{ m s}^{-1}$  and  $20 \text{ m s}^{-1}$ , corresponding to the chord-based Reynolds numbers  $Re_c$  ranging between  $0.8 \times 10^5$  and  $1.6 \times 10^5$ , respectively. The background noise is measured with an empty test section and all of the other parameters are otherwise identical, including the insertion of a turbulence-generation device upstream of the airfoil.

The absolute and relative noise spectra emitted by the baseline airfoil and its serrated and porous variants are shown in Fig. 3 for an angle of attack  $\alpha = 0^\circ$ . The reference sound pressure is  $p_{\text{ref}} = 20 \mu\text{Pa}$ . The free-stream velocity is set to  $U_\infty = 20 \text{ m s}^{-1}$  for the clean inflow and rod-airfoil configuration, whereas it is lowered to  $U_\infty = 14 \text{ m s}^{-1}$  ( $Re_c = 1.1 \times 10^5$ ) using the coarse turbulence-generation grid case resulting from the high blockage introduced by the latter.

It appears that the different airfoils introduce only a small noise contribution for the clean inflow condition. The airfoil self-noise is, indeed, known to be a relatively weak source mechanism. This is seen to be more significant for the porous airfoil because of the increase in the boundary layer turbulence intensity caused by the surface roughness. Much higher signal-to-noise ratios are obtained when the cylindrical rod and coarse grid are installed upstream of the airfoil, although those elements introduce a significant background of their own. The microphone signals have been processed as explained in Sec. III.C to isolate the airfoil noise.

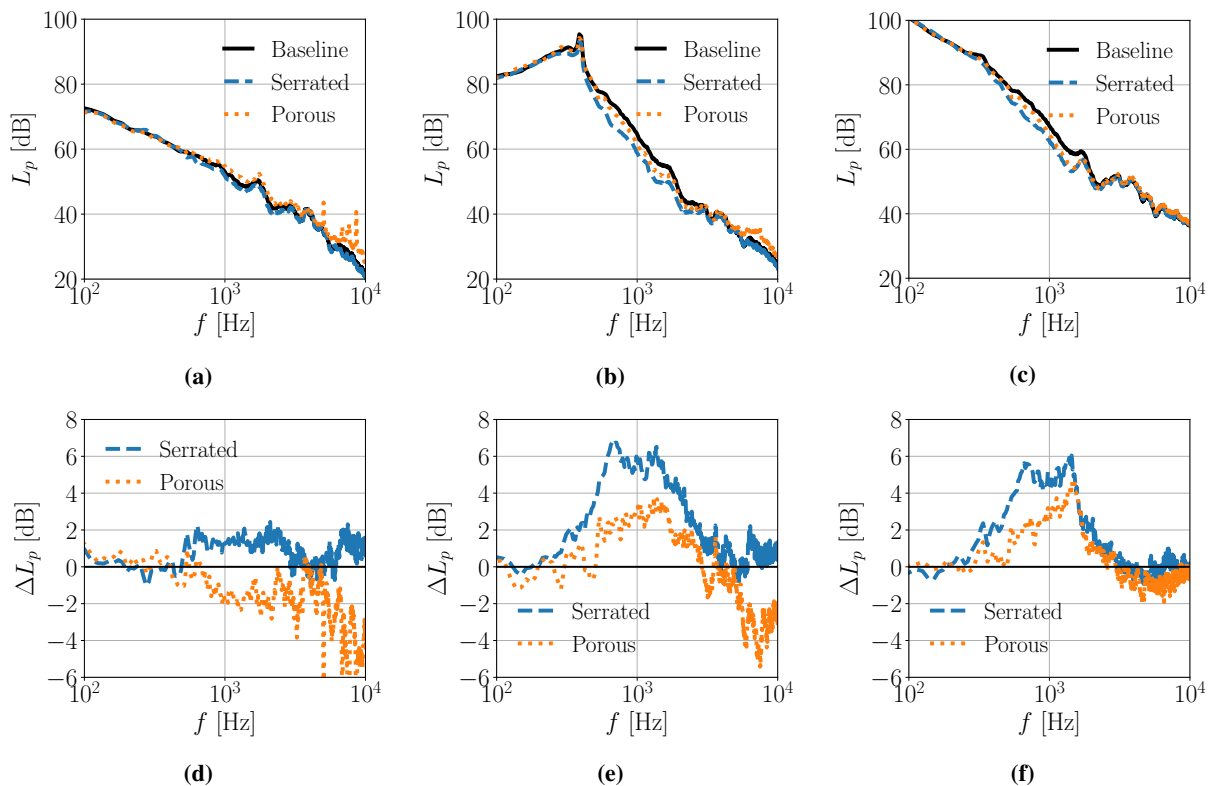


**Fig. 3** Absolute (top) and relative (bottom) SPL ( $p_{\text{ref}} = 20 \mu\text{Pa}$ ) emitted by the baseline, serrated, and porous airfoils for the different inflow conditions: (a,d) clean, (b,e) rod turbulence, (c,f) grid turbulence.  $\alpha = 0^\circ$  and  $U_\infty = 20 \text{ m s}^{-1}$  (clean, rod turbulence) and  $14 \text{ m s}^{-1}$  (grid turbulence). The regions of the plots that lie below the background noise level are highlighted in gray. A positive  $\Delta L_p$  indicates a noise reduction, whereas a negative  $\Delta L_p$  denotes noise increase.

**Serrations and porous materials** The noise attenuation  $\Delta L_p$  obtained with the serrated and porous airfoils are presented in Figs. 3d-3f. Assuming an auditory level discrimination threshold of 1 dB in ideal conditions, the results indicate that the noise differences provided by the two technologies should be just audible for the clean inflow conditions and quite audible for the rod-induced and grid-induced turbulent inflows. Noteworthy, the porosity increases the

self-noise over the entire frequency range in the clean inflow conditions and requires the incoming turbulence to yield the benefits. However, even in that case, relatively significant self-noise regeneration is found at the high frequencies.

The serrated airfoil model is the most effective in terms of the noise-reduction performance, reaching  $\Delta L_p = +6.5$  dB in the rod-airfoil case, followed by the porous model with a maximum reduction of  $\Delta L_p = +4.5$  dB with the grid turbulence. The serrations yield positive deviations in all of the considered configurations, although for  $f > 2$  kHz, the data are contaminated by the background noise.

**RVGs** The airfoil equipped with RVGs is compared with the baseline airfoil. The aeroacoustic spectra are presented in Fig. 4a for an angle of attack  $\alpha = 0^\circ$ . The results show that the RVGs introduce a noise increase at the high frequencies for  $f > 2$  kHz, which vanishes around  $f = 10$  kHz due to the predominance of the background noise. The increase in noise at the high frequencies can be the result of two factors. First, the trailing-edge noise is enhanced by the additional turbulence, which is generated and scattered. Second, at the higher frequencies, the noise generated by the RVGs themselves can become dominant. It has not been possible to highlight the expected benefit of delaying the separation, presumably because of the high blockage introduced with a high angle of attack and the influence of the side walls of the test section.

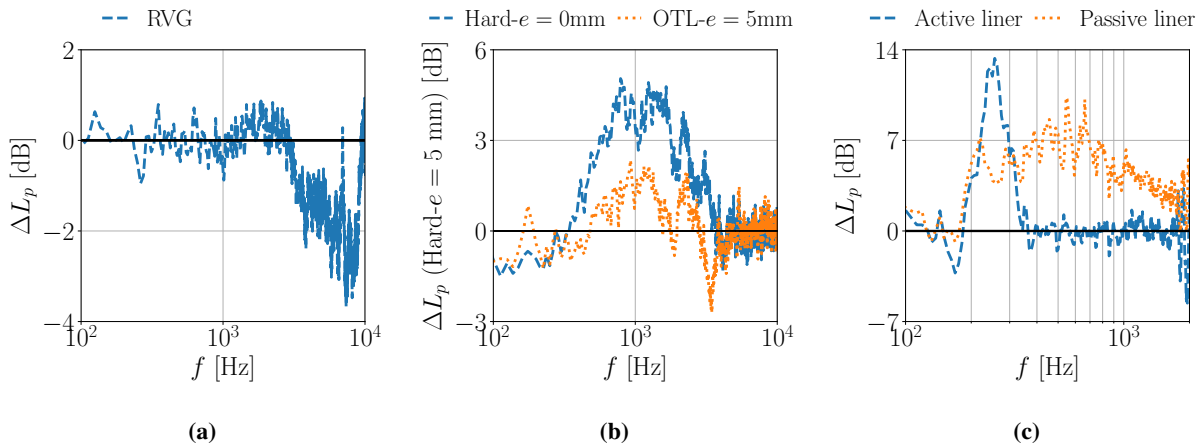


**Fig. 4** Noise alteration of (a) an airfoil equipped with RVGs relative to the baseline at  $U_\infty = 15 \text{ m s}^{-1}$  and  $\alpha = 0^\circ$  and in the absence of inflow turbulence, (b) the tip-gap noise configurations relative to an airfoil with a side gap  $e = 5$  mm at  $U_\infty = 10 \text{ m s}^{-1}$ ,  $\alpha = 9^\circ$  and in the absence of inflow turbulence, (c) the noise propagated along the wind tunnel treated with active and passive liners relative to a baseline solid panel.

**OTL** The tests have been carried at a free-stream velocity  $U_\infty = 10 \text{ m s}^{-1}$  and angle of attack  $\alpha = 9^\circ$  to assess the effectiveness of the liners for the tip-gap noise mitigation. These conditions induce a large enough pressure difference between the suction and pressure sides to yield the tip-gap noise with a side gap of  $e = 5$  mm between the airfoil and wall. Figure 4b shows the relative SPL levels  $\Delta L_p$  with reference to the gap airfoil with the solid wall case. The same convention is applied as was used for the previous results with the negative and positive values denoting a noise increase and reduction, respectively. Due to the higher noise levels expected on the pressure side of the airfoil and source being located at the mid chord [43], the results included in this section are obtained with the microphone closest to the gap side in correspondence with the leading edge on the tunnel wall facing the pressure side of the wing profile. The presence of a gap on the side of the airfoil introduces noise penalization, which gets particularly evident reaching 5 dB around  $f = 1$  kHz. The installation of a liner mitigates this penalization in a frequency band centered at  $f = 1$  kHz, recovering almost 2 dB at  $f = 800$  Hz. The results at  $f > 2$  kHz are contaminated by the background noise.

## B. Noise-propagation reduction

The rod-airfoil configuration is used to assess the effectiveness of the two liner technologies aimed at reducing the duct-noise propagation. The noise measured in the test section is amplified and reinjected through the loudspeaker facing the straight outlet duct. The results are shown in Fig. 4c. The passive liner proves to be quite efficient in a broad

frequency range between 200 Hz and 4 kHz with peaks of  $\Delta L_p > +7$  dB around 500 Hz. The active liner presents a noise reduction of  $\Delta L_p = +13$  dB in a narrower frequency band between 200 and 300 Hz, which can be tuned through the controller. This result highlights the potential of combining the two technologies. Overall, the achieved noise reductions allow an audience located at the outlet to hear the pronounced differences. This is also supported by the fact that the noise source can be band-filtered by the operator to isolate the frequency range of the maximum effectiveness of each technology.

### C. Noise-transmission reduction

A clean inflow is considered to investigate the effectiveness of the architected metamaterials, and the noise emitted in the test section is amplified through the main duct downstream. The transmitted acoustic spectrum shown in Fig. 5

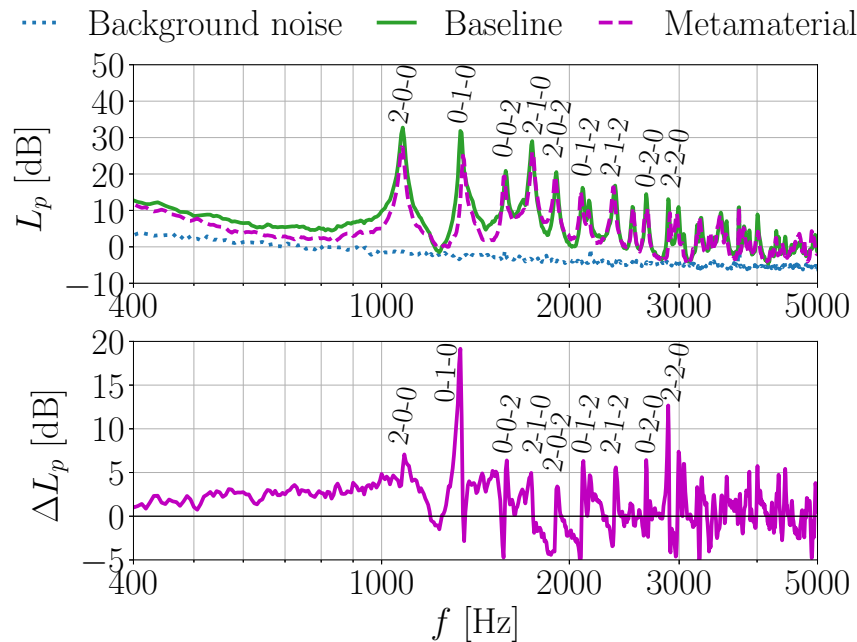


**Fig. 5 Absolute and relative SPL ( $p_{\text{ref}} = 20 \mu\text{Pa}$ ) spectra of the measurements on metamaterials for noise transmission. The modes  $n_x$ ,  $n_y$ , and  $n_z$  corresponding to each peak of the SPL spectra are marked,  $x$ ,  $y$ , and  $z$  coordinates being aligned as shown in Fig. 1.**

(top) appears to be dominated by the characteristic tonal peaks, which are linked to the acoustic modes of the backing cavity. Only the modes for which the location of the microphones does not lie on a node appear in the spectrum.  $\Delta L_p$  is consistently positive at the low frequencies for  $f < 1$  kHz with the most substantial reductions taking place for the targeted first axial mode, which is developing perpendicularly to the transmission panel. In the whole spectrum, the positive peaks of  $\Delta L_p$  correspond to the excitation modes. The frequency misalignment of the tonal peaks between the two cases is probably due to the slight differences introduced to the dimensions of the cavity by the transmission panel in use. In this case, a set of headphones will be installed along with the microphone to allow the users to perceive the noise propagated through the backing cavity.

## V. Conclusions

A didactic demonstrator has been designed as an open-loop miniature aeroacoustic wind tunnel, aimed at illustrating, in an audible fashion, the different flow-induced noise mechanisms on the one hand and demonstrating the effectiveness of the advanced technologies to attenuate them on the other hand. The noise-mitigation strategies have been investigated, modeled, and fine-tuned for this demonstrator by the young researchers of the European Marie Skłodowska Curie ITN SMARTANSWER for the reduction of sound generation at the source, its propagation in a duct, and its transmission

through a structural panel.

The design procedure combines the classical elements of a low-noise and low-turbulence wind tunnel with the specific features that enhance a didactic and live audio experience. A turbulence intensity on the order of 0.5 % in clean inflow conditions has been achieved, and the acoustic signal-to-noise ratio of the test airfoil has been found satisfactory as well.

The demonstrator was shown to provide an audible experience of the performance of the noise-mitigation technologies. These effects occur at the frequencies covering the relevant human hearing range and show amplitudes that are mainly above the hearing discrimination threshold. Therefore, a potential user standing near the outlet of the wind tunnel can experience the effectiveness of the serrations, porous materials, and OTLs at the mid-range frequencies and noise generation of the RVGs at the high frequencies. The passive liners provide clear broadband mitigation during the propagation, whereas the active liners offer even more substantial reductions over a narrower frequency band. Finally, the metamaterials dampen, quite effectively, the acoustic transmission through a flexible panel. An interface has been developed to enhance the user's perception of such technologies by applying the bandpass filters to the noise source to isolate the frequency bands of the maximum effectiveness.

The measured noise alterations of the different technologies agree with the literature, highlighting the suitability of the demonstrator for the small-scale, yet quantitative, aeroacoustic research. The facility will serve as a practical test bench for future students and can be put at the disposal of partners wishing to test cheap three-dimensionally printed test airfoils and/or model related noise-generation or attenuation mechanisms.

To conclude, the demonstrator appears to be suitable to address an audience across a broad range of education or expertise levels. It enables the explanations that are accessible to primary and secondary school students and will, hopefully, trigger interest in scientific studies. It also gives graduate students the possibility of setting up preliminary experiments independently and familiarizing themselves with the high levels of accuracy required by the acoustic measurements in the laboratory. It is, thus, expected that this facility will continue to be upgraded and serve future research in aeroacoustics. Finally, the technologies demonstrated are of large socioeconomical relevance, which should help to reconnect the layman with the technological progress and scientific policies in particular.

### Acknowledgments

The authors acknowledge the support of the European Commission, through the H2020 Marie Skłodowska-Curie ITN "SMARTANSWER - Smart mitigation of flow-induced acoustic radiation and transmission" Grant No. 722401. The authors are very grateful to EBM-Papst for having graciously offered the centrifugal fan used in the demonstrator. Finally, the following Early Stage Researchers of SMARTANSWER have contributed to the investigation of the noise reduction reported in this paper and must be thanked: Felipe Alves Pires (Katholieke Universiteit Leuven), Emanuele De Bono and Georgios Bampanis (École Centrale de Lyon), Massimo Emiliano D'Elia (Laboratoire d'Acoustique de l'Université du Maine), Ignacio Zurbano-Fernández (Technical Center Industries Aérauliques Et Thermiques), Niloofar Sayyad Khoashenas (KTH Royal Institute of Technology), Lourenco Lima Pereira, Christopher Teruna (Delft University of Technology), Sergi Pallejà Cabré (University of Southampton), and Tanushree Suresh (Polish Academy of Science).

### References

- [1] Tamaro, S., Zamponi, R., and Schram, C., "Development of a didactic demonstrator for flow-induced noise mechanisms and mitigation technologies," *Journal of Acoustical Society of America*, Vol. 151, 2022, p. 898. <https://doi.org/10.1121/10.0009366>.
- [2] Hawkinson, D., and Anderson, M., "A novel approach to student programs and pre-college outreach - The Iowa State University Flight Demonstration Wind Tunnel," *39th Aerospace Sciences Meeting and Exhibit*, 2001. <https://doi.org/10.2514/6.2001-8>.
- [3] Duran, J. R., Whidborne, J. F., Carrizales, M., and Pontillo, A., "A benchtop flight control demonstrator," *International Journal of Mechanical Engineering Education*, Vol. 49, No. 1, 2021, pp. 80–97. <https://doi.org/10.1177/0306419019852688>, URL <https://doi.org/10.1177/0306419019852688>.
- [4] Schram, C. (ed.), *Advanced concepts for the reduction of flow-induced noise generation, propagation and transmission*, VKI LS 2021-01, von Karman Institute, Rhode-St-Genève, 2020.
- [5] Bampanis, G., Roger, M., Ragni, D., Avallone, F., and Teruna, C., "Airfoil-Turbulence Interaction Noise Source Identification and its Reduction by Means of Leading Edge Serrations," *25th AIAA/CEAS Aeroacoustics Conference*, AIAA, Delft, NL, 2018. <https://doi.org/10.2514/6.2019-2741>.

- [6] Bampanis, G., Roger, M., and Moreau, S., “On a three-dimensional investigation of airfoil turbulence-impingement noise and its reduction by leading-edge tubercles,” *Journal of Sound and Vibration*, Vol. 520, 2022, p. 116635. <https://doi.org/10.1016/j.jsv.2021.116635>.
- [7] Subramanian, N., Paruchuri, C., Haeri, S., Joseph, P., Kim, J. W., and Polacsek, C., “Airfoil noise reductions through leading edge serrations,” *Physics of Fluids*, Vol. 27, 2015, p. 025109. <https://doi.org/10.1063/1.4907798>.
- [8] Kim, J. W., Haeri, S., and Joseph, P. F., “On the reduction of aerofoil-turbulence interaction noise associated with wavy leading edges,” *Journal of Fluid Mechanics*, Vol. 792, 2016, p. 526–552. <https://doi.org/10.1017/jfm.2016.95>.
- [9] Paruchuri, C., Joseph, P., Narayanan, S., Vanderwel, C., Turner, J., Kim, J. W., and Ganapathisubramani, B., “Performance and mechanism of sinusoidal leading edge serrations for the reduction of turbulence-aerofoil interaction noise,” *Journal of Fluid Mechanics*, Vol. 818, 2017, pp. 435–464. <https://doi.org/10.1017/jfm.2017.141>.
- [10] Lima Pereira, L., Ragni, D., Avallone, F., and Scarano, F., “Pressure fluctuations from large-scale PIV over a serrated trailing edge,” *Experiments in Fluids: experimental methods and their applications to fluid flow*, Vol. 61, No. 3, 2020, p. 71. <https://doi.org/10.1007/s00348-020-2888-x>.
- [11] Avallone, F., van der Velden, W. C. P., Ragni, D., and Casalino, D., “Noise reduction mechanisms of sawtooth and combed-sawtooth trailing-edge serrations,” *Journal of Fluid Mechanics*, Vol. 848, 2018, p. 560–591. <https://doi.org/10.1017/jfm.2018.377>.
- [12] Teruna, C., Manegar, F., Avallone, F., Casalino, D., Ragni, D., Rubio Carpio, A., and Carolus, T., “Numerical Analysis of Metal-Foam Application for Trailing Edge Noise Reduction,” *25th AIAA/CEAS Aeroacoustics Conference*, American Institute of Aeronautics and Astronautics Inc. (AIAA), Delft, NL, 2019. <https://doi.org/10.2514/6.2019-2650>.
- [13] Teruna, C., Manegar, F., Avallone, F., Ragni, D., Casalino, D., and Carolus, T., “Noise reduction mechanisms of an open-cell metal-foam trailing edge,” *Journal of Fluid Mechanics*, Vol. 898, 2020, p. A18. <https://doi.org/10.1017/jfm.2020.363>.
- [14] Teruna, C., Avallone, F., Ragni, D., and Casalino, D., “On the noise reduction of a porous trailing edge applied to an airfoil at lifting condition,” *Physics of Fluids*, Vol. 33, No. 5, 2021, p. 055132. <https://doi.org/10/gk5f3z>.
- [15] Bampanis, G., and Roger, M., “On the Turbulence-Impingement Noise of a NACA-12 Airfoil with Porous Inclusions,” *26th AIAA/CEAS Aeroacoustics Conference*, AIAA, VIRTUAL EVENT, 2020. <https://doi.org/10.2514/6.2020-2577>.
- [16] Zamponi, R., Ragni, D., Wyer, N., and Schram, C., “Experimental Investigation of Airfoil Turbulence-Impingement Noise Reduction Using Porous Treatment,” *25th AIAA/CEAS Aeroacoustics Conference*, AIAA, Delft, NL, 2019. <https://doi.org/10.2514/6.2019-2649>.
- [17] Zamponi, R., Satcunanathan, S., Moreau, S., Ragni, D., Meinke, M., Schröder, W., and Schram, C., “On the role of turbulence distortion on leading-edge noise reduction by means of porosity,” *Journal of Sound and Vibration*, Vol. 485, 2020, p. 115561. <https://doi.org/10.1016/j.jsv.2020.115561>.
- [18] Zamponi, R., “Investigation of turbulence-surface interaction noise mechanisms and their reduction using porous materials,” Ph.D. thesis, Delft University of Technology, Apr. 2021. <https://doi.org/10.4233/uuid:d332c7e3-87be-4ed6-aa71-e629ef77e07a>.
- [19] Zamponi, R., Moreau, S., and Schram, C., “Rapid distortion theory of turbulent flow around a porous cylinder,” *Journal of Fluid Mechanics*, Vol. 915, 2021, p. A27. <https://doi.org/10.1017/jfm.2021.8>.
- [20] Paruchuri, C., Joseph, P., Chong, T., Priddin, M., and Ayton, L., “On the noise reduction mechanisms of porous aerofoil leading edges,” *Journal of Sound and Vibration*, 2020. <https://doi.org/10.1016/j.jsv.2020.115574>.
- [21] Rubio Carpio, A., Merino Martínez, R., Avallone, F., Ragni, D., Snellen, M., and van der Zwaag, S., “Experimental characterization of the turbulent boundary layer over a porous trailing edge for noise abatement,” *Journal of Sound and Vibration*, Vol. 443, 2019, pp. 537–558. <https://doi.org/10.1016/j.jsv.2018.12.010>.
- [22] Palleja-Cabre, S., Tester, B. J., Jeremy Astley, R., and Bampanis, G., “Aeroacoustic Assessment of Performance of Overtip Liners in Reducing Airfoil Noise,” *AIAA Journal*, Vol. 59, No. 9, 2021, pp. 3622–3637. <https://doi.org/10.2514/1.J060134>.
- [23] Amoiridis, O., Zarri, A., Zamponi, R., Pasco, Y., Yakhina, G., Christophe, J., Moreau, S., and Schram, C., “Sound localization and quantification analysis of an automotive engine cooling module,” *Journal of Sound and Vibration*, Vol. 517, 2022, p. 116534. <https://doi.org/10.1016/j.jsv.2021.116534>.
- [24] Palleja-Cabre, S., Tester, B. J., and Astley, R. J., “Modelling of ducted noise sources in the proximity of acoustic liners,” *Journal of Sound and Vibration*, Vol. 517, 2022, p. 116548. <https://doi.org/10.1016/j.jsv.2021.116548>.

- [25] Martinez Suarez, J., Flaszynski, P., and Doerffer, P., “Application of rod vortex generators for flow separation reduction on wind turbine rotor,” *Wind Energy*, Vol. 21, No. 11, 2018, pp. 1202–1215. <https://doi.org/10.1002/we.2224>.
- [26] Hansen, M., Velte, C., Øye, S., Hansen, R., Sørensen, N., Madsen, J., and Mikkelsen, R., “Aerodynamically shaped vortex generators,” *Wind Energy*, Vol. 19, No. 3, 2016, p. 563–567. <https://doi.org/10.1002/we.1842>.
- [27] Doerffer, P., Flaszynski, P., and Szwaba, R., “Streamwise vortex generator,” , 11 2009. Patent application PL389685.
- [28] Boulandet, R., Lissek, H., Karkar, S., Collet, M., Matten, G., Ouisse, M., and Versaevel, M., “Duct modes damping through an adjustable electroacoustic liner under grazing incidence,” *Journal of Sound and Vibration*, Vol. 426, 2018, pp. 19–33. <https://doi.org/10.1016/j.jsv.2018.04.009>.
- [29] Billon, K., Bono, E. D., Perez, M., Salze, E., Matten, G., Gillet, M., Ouisse, M., Volery, M., Lissek, H., Mardjono, J., and Collet, M., “Experimental assessment of an active (acoustic) liner prototype in an acoustic flow duct facility,” *Health Monitoring of Structural and Biological Systems XV*, Vol. 11593, SPIE, VIRTUAL EVENT, 2021, pp. 505 – 511. <https://doi.org/10.1117/12.2583099>.
- [30] Davern, W., “Perforated facings backed with porous materials as sound absorbers — An experimental study,” *Applied Acoustics*, Vol. 10, No. 2, 1977, pp. 85–112. [https://doi.org/10.1016/0003-682X\(77\)90019-6](https://doi.org/10.1016/0003-682X(77)90019-6).
- [31] Pires, F. A., Claeys, C., Deckers, E., and Desmet, W., “The impact of resonant additions’ footprint on the stop band behavior of 1D locally resonant metamaterial realizations,” *Journal of Sound and Vibration*, Vol. 491, 2021, p. 115705. <https://doi.org/10.1016/j.jsv.2020.115705>.
- [32] Alves Pires, F., Sangiuliano, L., Denayer, H., Deckers, E., Claeys, C., and Desmet, W., “Suppression of flow-induced noise and vibrations by locally resonant metamaterials,” *26th AIAA/CEAS Aeroacoustics Conference*, AIAA, VIRTUAL EVENT, 2020, pp. 2586–2594. <https://doi.org/10.2514/6.2020-2586>.
- [33] Claeys, C., Rocha de Melo Filho, N. G., Van Belle, L., Deckers, E., and Desmet, W., “Design and validation of metamaterials for multiple structural stop bands in waveguides,” *Extreme Mechanics Letters*, Vol. 12, 2017, pp. 7–22. <https://doi.org/10.1016/j.eml.2016.08.005>.
- [34] ebm-papst Mulfingen GmbH & Co., *EC centrifugal fan - RadiPac Datasheet*, 5 2007.
- [35] Jacob, M., Boudet, J., Casalino, D., and Michard, M., “A rod-airfoil experiment as a benchmark for broadband noise modeling,” *Theoretical and Computational Fluid Dynamics*, Vol. 19, 2005, pp. 171–196. <https://doi.org/10.1007/s00162-004-0108-6>.
- [36] Gruber, M., Joseph, P., and Chong, T., “On the mechanisms of serrated airfoil trailing edge noise reduction,” *17th AIAA/CEAS Aeroacoustics Conference*, AIAA, Portland, OR, 2011. <https://doi.org/10.2514/6.2011-2781>.
- [37] Howe, M. S., “Noise produced by a sawtooth trailing edge,” *The Journal of the Acoustical Society of America*, Vol. 90, No. 1, 1991, pp. 482–487. <https://doi.org/10.1121/1.401273>.
- [38] Teruna, C., Avallone, F., Casalino, D., and Ragni, D., “Numerical Investigation of Leading Edge Noise Reduction on a Rod-Airfoil Con-figuration Using Porous Materials and Serrations,” *Journal of Sound and Vibration*, Vol. 494, 2020. <https://doi.org/10.1016/j.jsv.2020.115880>.
- [39] Rubio Carpio, A., Avallone, F., Ragni, D., Snellen, M., and van der Zwaag, S., “3D-printed Perforated Trailing Edges for Broadband Noise Abatement,” *25th AIAA/CEAS Aeroacoustics Conference*, AIAA, Delft, NL, 2019. <https://doi.org/10.2514/6.2019-2458>.
- [40] Guess, A., “Calculation of perforated plate liner parameters from specified acoustic resistance and reactance,” *Journal of Sound and Vibration*, Vol. 40, No. 1, 1975, pp. 119–137. [https://doi.org/10.1016/S0022-460X\(75\)80234-3](https://doi.org/10.1016/S0022-460X(75)80234-3).
- [41] Curle, N., “The influence of solid boundaries upon aerodynamic sound,” *Proceedings of the Royal Society of London. Series A. Mathematical and Physical Sciences*, Vol. 231, No. 1187, 1955, pp. 505–514. <https://doi.org/10.1098/rspa.1955.0191>.
- [42] Jacobsen, F., Poulsen, T., Rindel, J., Gade, A., and Ohlrich, M., *Fundamentals of Acoustics and Noise Control*, Technical University of Denmark, Department of Electrical Engineering, Kongens Lyngby, DK, 2011.
- [43] Koch, R., Sanjosé, M., and Moreau, S., “Large-Eddy Simulation of a Single Airfoil Tip-Leakage Flow,” *AIAA Journal*, Vol. 59, No. 7, 2021, pp. 2546–2557. <https://doi.org/10.2514/1.J060057>.